Supporting Information:

Switchable optical trapping based on vortex-pair beams generated by a polarization-multiplexed dielectric metasurface

Hongliang Li,[a,b] Jisen Wen,*[c] Song Gao,[d] Duk-Yong Choi,[e] Jin Tae Kim,[f] and Sang-Shin Lee*[a,b]

[a]Department of Electronic Engineering, Kwangwoon University, Seoul, 01897, South Korea

[b]Nano Device Application Center, Kwangwoon University, Seoul, 01897, South Korea

[c]Research Center for Intelligent Chips and Devices, Zhejiang Lab, Hangzhou, 311121, China

[d]School of Information Science and Engineering, Shandong Provincial Key Laboratory of Network-based Intelligent Computing, University of Jinan, Jinan, Shandong, 250022, China

[e]Department of Quantum Science and Technology, Research School of Physics, Australian National University, Canberra, ACT 2601, Australia

[f]Quantum Technology Research Department, Electronics and Telecommunications Research Institute, Daejeon, 34129, South Korea

*Corresponding authors' e-mail addresses:

wenjisen@zju.edu.cn (Jisen Wen); slee@kw.ac.kr (Sang-Shin Lee)

S1: Optical transfer characteristics of the nanopost meta-atoms

The transmission amplitude (T) and phase shift (φ) of the nanopost meta-atoms were calculated for both transverse electric (TE) and transverse magnetic (TM) polarizations using the FDTD (finite-difference time-domain) Solutions, as depicted in Figures S1(a) and S1(b), respectively. To embody the proposed metasurface, an ensemble of 8 × 8 meta-atoms have been selected out of the TiO_2 nanopost candidates whose cross-sectional dimensions (w and l) range from 70 to 270 nm, marked by black star symbols. The selected meta-atoms were confirmed to induce a complete 2π phase shift for both TE and TM polarizations and give rise to an average transmittance exceeding 0.8 for normal incident light.
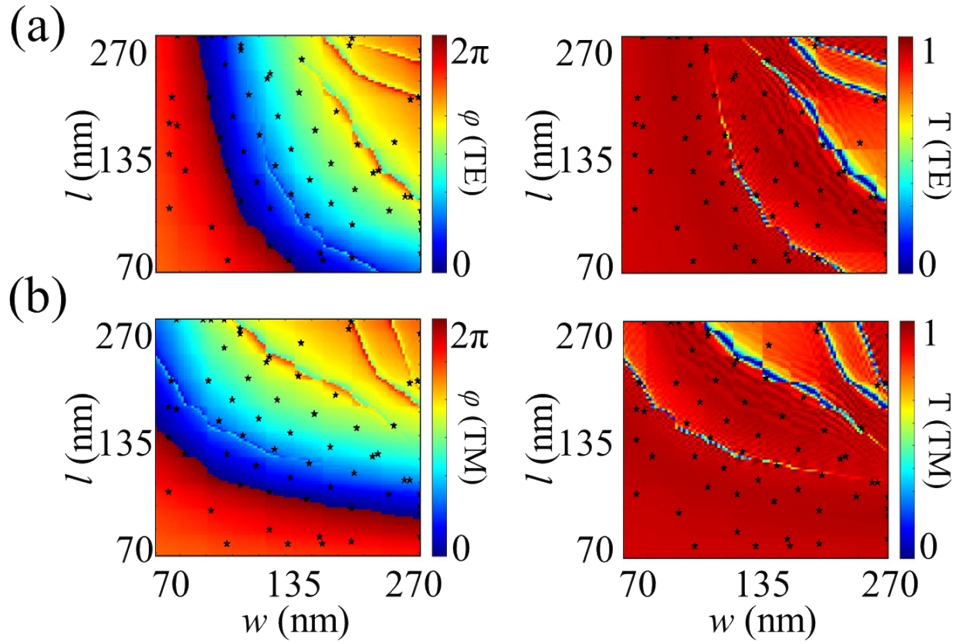

Fig. S1 Optical characteristics of the meta-atoms. Simulated optical transmission T and phase shift φ of the nanoposts in terms of the cross-sectional dimensions of w and l under normally incident (a) TE- and (b) TM-polarized beam conditions with a fixed height of h = 500 nm and a period p= 350 nm. Black star symbols represent the selected meta-atoms.

S2: Relationship between the phase profiles of vortex pairs and their design parameters

To select appropriate parameters pertaining to the metasurface that lead to the desired optical trapping function, the phase profile of the vortex pair was assessed in four different cases. The spot size (d) of the incident Gaussian beam was equal to the diameter of the metasurface, which was 93 μm. First, as shown in Figure S2(a), the vortex-pair phase was calculated by altering m_2 from one to six, with $a = m_1 = 0$. The phase profile of the vortex-pair beam led to a single-phase singularity, as in the case of the vortex phase profile. For $a = 0$ and m_1 (m_2) (taking values from one to six), the phase profiles emulated the behavior of a single vortex, as depicted in Figure S2(b). This phenomenon arises because the two vortex-phase singularities overlap, resulting in an observable topological charge equivalent to $m_1 + m_2$. Meanwhile, to maintain a proper distance between the two particles during the optical trapping, another six cases of off-axis distances, including a in the range of 0 to 0.25 × d with

intervals of 0.05 × d, were considered and analyzed as shown in Figure S2(c). As depicted in Figure S2(d), although the two topological charges can assume different values, the asymmetry in terms of the phase profile may affect the electric field distribution and the resulting trapping characteristics. For example, two distinct representative cases were selected to validate the simulation results, as depicted in Figure S2(e). Considering the electric field distributions of the two cases, $m_1 = 1$, $m_2 = -3$ and $m_1 = 1$, $m_2 = 3$, with the same numerical value but different topological charges (see Figure 3(d)), it was asserted that there existed only a single bright spot in the case of $m_1 = 1$, $m_2 = -3$; by contrast, there were two bright spots in the case of $m_1 = 1$, $m_2 = 3$, which is similar to the case in which the vortex-pair beam exhibits the same absolute topological charge value. When the values of the two topological charges are not the same, however, the phase profiles of the two vortices will be noticeably differentiated from each other. This indicates that the phase variation within the light beam will exhibit distinct characteristics that differ from the case of typical helical patterns associated with the orbital angular momentum. As a result of these differences in the phase profile, the properties of the beam may be altered in terms of the optical forces and trapping behavior. Finally, to ensure that the designed metasurface can effectively fulfill its intended function, two sets of topological charges ($m_1 = 3$, $m_2 = -3$, $a = 14$ μm and $m_1 = 1$, $m_2 = 1$, $a = 14$ μm) were chosen.
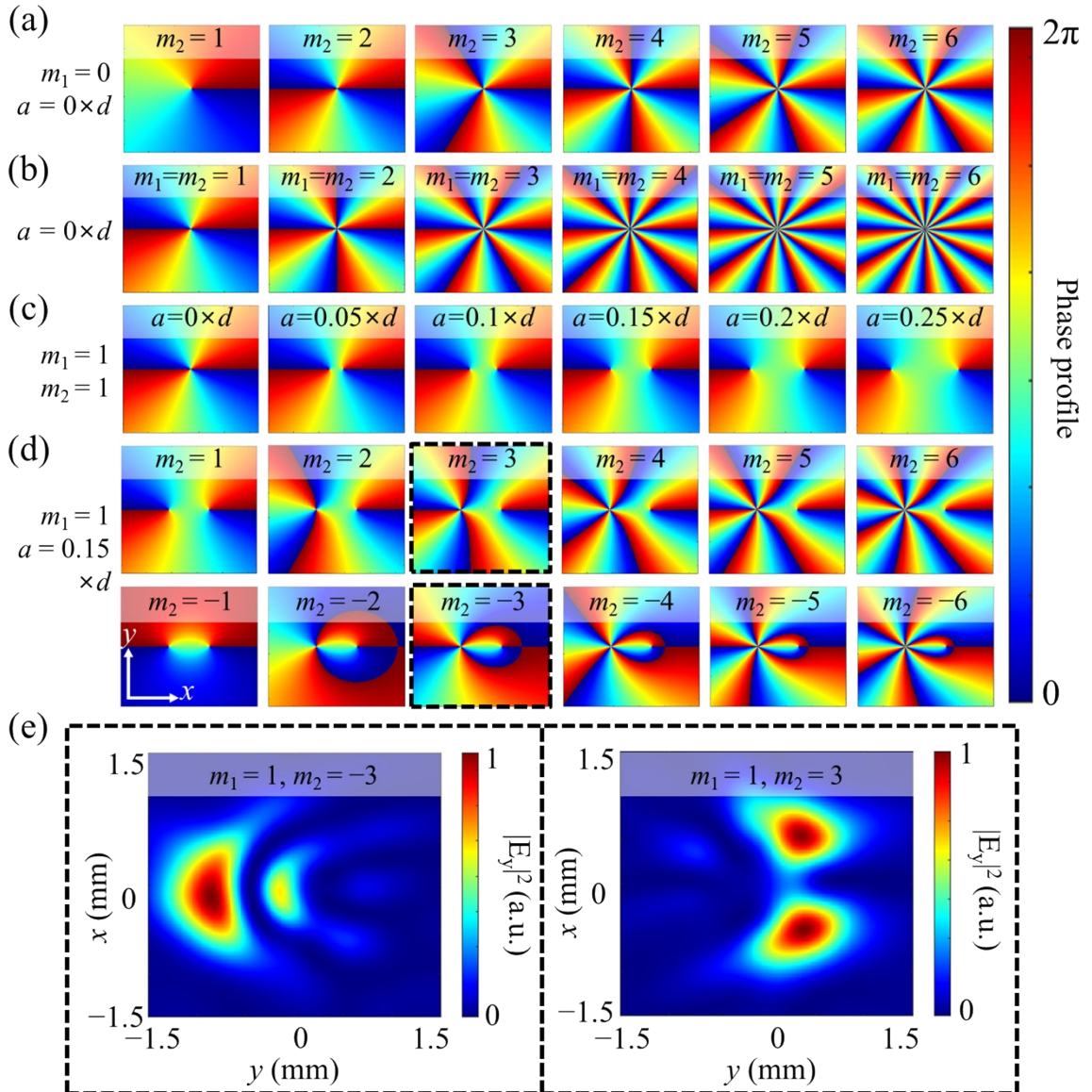
Fig. S2 Phase profiles of the vortex pairs in terms of their design parameters including m_1, m_2, and a. Four cases were sequentially investigated by varying (a) m_2, (b) m_1 and m_2, (c) a, and (d) m_2, with the rest of the parameters fixed. (e) Calculated far-field intensity profiles of the vortex-pair beams with topological charge combinations of $m_1 = 1$, $m_2 = -3$, and $m_1 = 1$, $m_2 = 3$.

S3: Effects of the spot sizes of incident Gaussian beams on the vortex-pair beam profiles

To examine the impacts of the diameters of the incident Gaussian beams on the vortex-pair beam, numerical simulations were performed. As presented in Figure S3, the impact of the vortex on the optical field distribution of the Gaussian beam, with radii ranging from a to $6a$, was mainly explored. Herein, a refers to the initial off-axis distance between the two vortices, which is equivalent to 14 μm. Figure S3(a) shows that under TE polarization conditions, the beam power gradually shifts toward the right and ultimately converges at the center of the spot at larger incident beam radius values. Under TM polarization conditions, as shown in Figure S3(b), the two intense spots initially appear to be linked to each other and begin to be set apart at increasing beam spots. With a larger distance between the two spots, their intensities are escalated to evolve eventually into two separate beams. These results provide valuable insights into the influences of the incident beam size on the field profile associated with the vortex-pair beam.
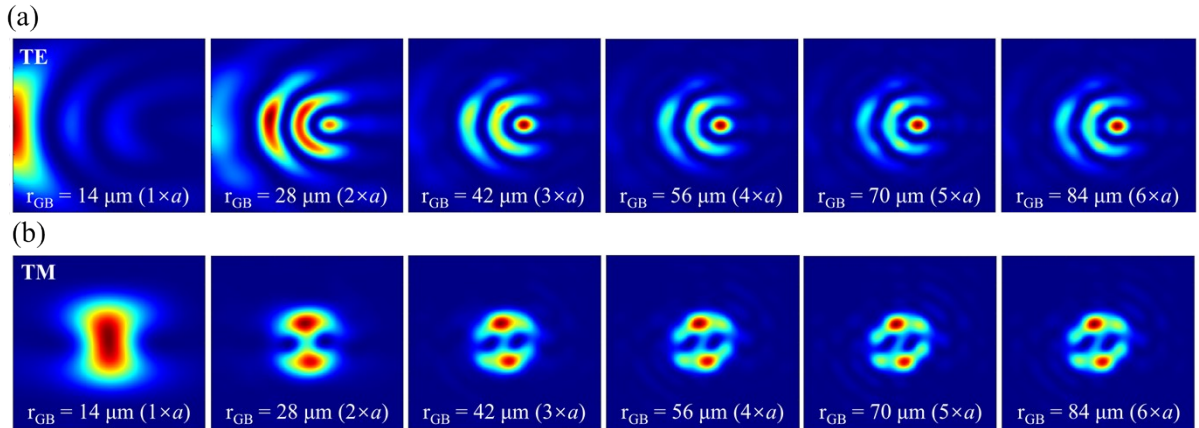
(a)

(b)

Fig. S3 Effects of the Gaussian beam radius (r_{GB}, varying from 14 to 84 μm at 14 μm intervals) on the simulated vortex-pair beam profiles in the (a) TE and (b) TM cases.

S4: Vortex-pair beam-mediated optical trapping of dielectric microbeads

For an optical tweezer, the principal mechanism of manipulating particles derives from the gradient (F_g) and scattering forces (F_s).[1–3] Conventional, focused Gaussian beam-based optical tweezers often rely on a gradient force to confine particles.[4,5] Regarding vortex beam-based optical trapping, a scattering force plays a prime role, which is known to induce the rotational motion of the particle, thus leading to the spinning thereof.[6,7] In the case of the proposed vortex-pair beam, the particles are believed to be predominantly trapped and firmly immobilized by the transverse gradient force, without invoking significant rotation driven by the weak orbital angular momentum.[8] As depicted in Figure S3(a), the dielectric microbeads are attracted toward the beam's center in the vicinity of the glass slide, in both cases of topological charges with the same or opposite signs. We attempted

4

to analyze the transverse optical trapping force from the perspective of the principle of fluid mechanics according to Stokes's law.[9] As shown in Figure S3(b), when the sample chamber was moved along the *x*- or *y*-axis, the microbeads in the suspension medium primarily succumbed to the viscous (F_{vis}) and transverse gradient forces. Herein, the transverse gradient force refers to the force exerted on the microbeads in the lateral direction, perpendicular to the beam propagation.[10,11] In the context of the proposed vortex-pair beam, the gradient force was primarily responsible for trapping and immobilization of the particles. The viscous force stems from the viscosity of the surrounding medium,[12,13] which is regarded as a resistive force that opposes the motion of the particles as they move through the fluid. In the case of optical trapping, the viscous force acts in conjunction with the transverse gradient force to control the movement and positioning of the trapped particles.[7] When the power at the beam waist is increased to 5 mW, the gradient force prevails over the viscous force so that the microbeads can be captured by the vortex and remain stationary. The sample plate should be moved at a sufficiently slow velocity (v_x and v_y) to limit the viscous force.
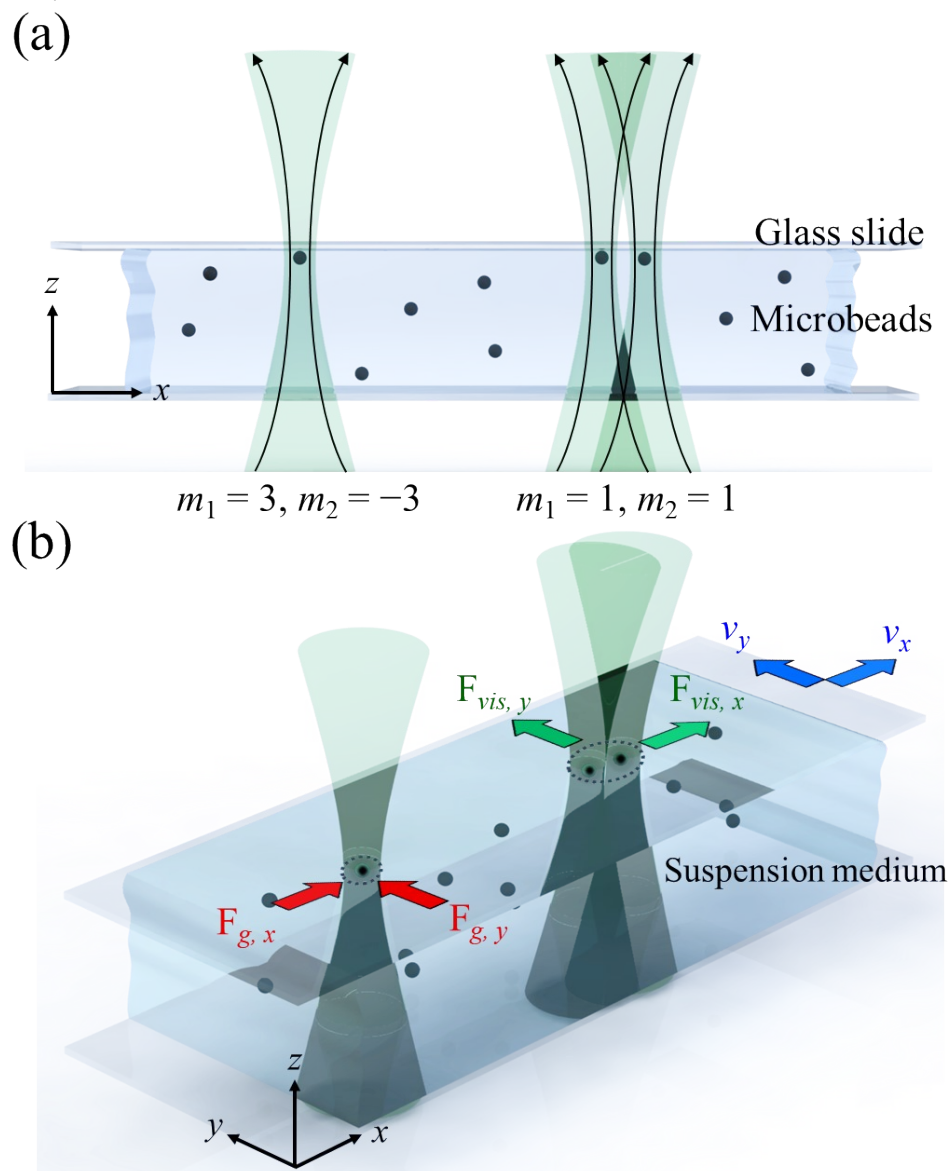

Fig. S4 (a) Front- and (b) side-views of the configuration of the proposed optical trapping scheme.

S5: Positional coordinates of the two strong beam spots corresponding to the two topological charges with the same sign
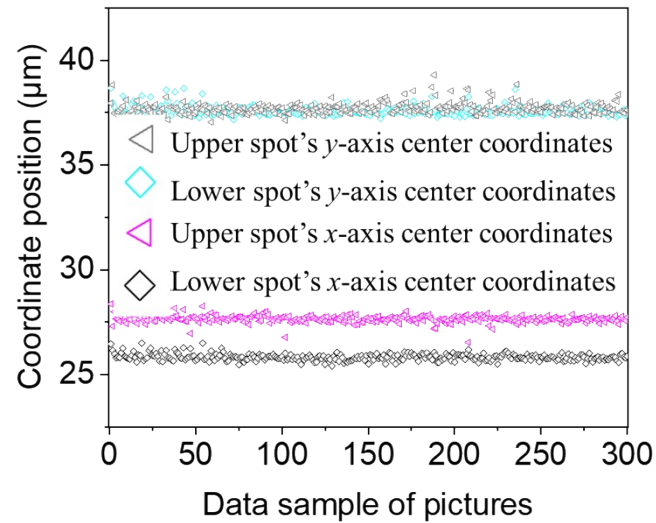

Fig. S5 *XY* center coordinates corresponding to the two strong spots in the vortex pair beam in the case of $m_1 = 1$, $m_2 = 1$.

S6: Evolution of vortex-pair beams from plane wave mode to tightly focused mode
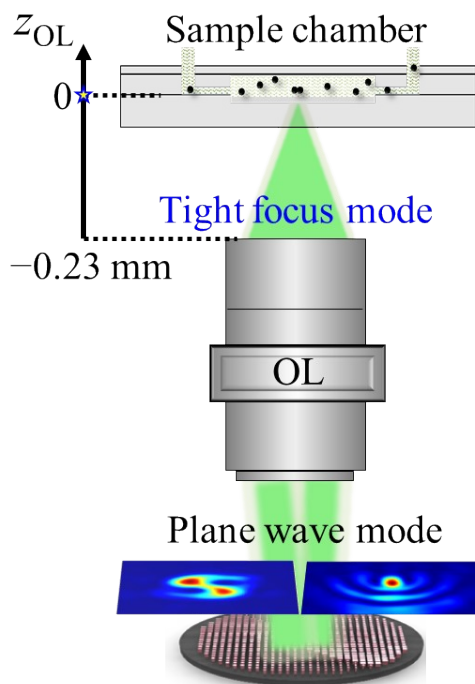

Fig. S6 Schematic of the evolution of vortex-pair beams from a plane wave mode to a tightly focused mode.

S7: Procedure used to fabricate the metasurface and its structural images
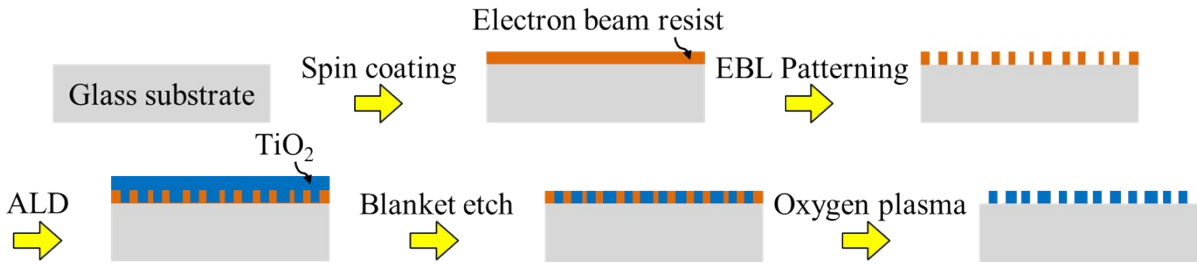
Fig. S7 Electron-beam lithography (EBL)-based fabrication process for the designed metasurface. (ALD: atomic layer deposition)

REFERENCES

1. M. Muradoglu, W. S. Y. Chiu, and T. W. Ng, Optical force lateral push–pulling using focus positioning. *J. Opt. Soc. Am. B*, 2012, **29**, 874–880.

2. M. Daly, M. Sergides, and S. N. Chormaic, Optical trapping and manipulation of micrometer and submicrometer particles. *Laser Photonics Rev.*, 2015, **9**, 309–329.

3. Y. Tian, L. Wang, G. Duan, and L. Yu, Multi-trap optical tweezers based on composite vortex beams. *Opt. Commun.*, 2021, **485**, 126712.

4. Y. Ren, Q. Chen, M. He, X. Zhang, H. Qi, and Y. Yan, Plasmonic optical tweezers for particle manipulation: principles, methods, and applications. *ACS Nano*, 2021, **15**, 6105–6128.

5. C. J. Bustamante, Y. R. Chemla, S. Liu, and M. D. Wang, Optical tweezers in single-molecule biophysics. *Nat. Rev. Methods Primers*, 2021, **1**, 25.

6. S. Cheng, S. Tao, C. Zhou, and L. Wu, Optical trapping of a dielectric-covered metallic microsphere. *J. Opt.*, 2015, **17**, 105613.

7. H. Xin, Y. Li, Y. C. Liu, Y. Zhang, Y. F. Xiao, and B. Li, Optical forces: from fundamental to biological applications. *Adv. Mater.*, 2020, **32**, 2001994.

8. J. Wen, B. Gao, G. Zhu, D. Liu, and L. G. Wang, Precise position and angular control of optical trapping and manipulation via a single vortex-pair beam. *Opt. Lasers Eng.*, 2022, **148**, 106773.

9. G. G. Stokes, On the effect of the internal friction of fluids on the motion of pendulums. *Pitt Press*, Cambridge Philosophical Society, 1851, **9**, 8–106.

10. P. Polimeno, A. Magazzu, M. A. Iati, F. Patti, R. Saija, C. D. E. Boschi, M. G. Donato, P. G. Gucciardi, P. H. Jones, G. Volpe, and O. M. J. Marago, Optical tweezers and their applications. *Quant. Spectrosc. Radiat. Transf.*, 2018, **218**, 131–150.

11. M. Daly, M. Sergides, and S. Nic Chormaic, Optical trapping and manipulation of micrometer and submicrometer particles. *Laser Photonics Rev.*, 2015, **9**, 309–329.

12. A. Yao, M. Tassieri, M. Padgett, and J. Cooper, Microrheology with optical tweezers. *Lab Chip*, 2009, **9**, 2568–2575.

13. C. J. Bustamante, Y. R. Chemla, S. Liu, and M. D. Wang, Optical tweezers in single-molecule biophysics. *Nat. Rev. Methods Primers*, 2021, **1**, 25.